Anal. Chem. **1999,** *71,* 574−581

Photoionization of Gas-Phase versus Ion-Beam-Desorbed Dopamine with Femtosecond Laser Pulses

Vasil Vorsa, Kenneth F. Willey, and Nicholas Winograd*

Department of Chemistry, 184 Materials Research Institute Building, The Pennsylvania State University, University Park, Pennsylvania 16802

We have investigated the photoionization of gas-phase and ion-beam desorbed dopamine using femtosecond laser pulses at wavelengths of 800, 400, 267, and 200 nm. Photoionization of gas-phase dopamine is found to produce the molecular ion, and three fragment ions at all four wavelengths, with the branching ratios strongly wavelength dependent. Photoionization at 400 and 267 nm yields the highest molecular ion signal, while that at 800 and 200 nm produces very little molecular ion signal. An excited-state lifetime of ∼10 ps following 267-nm excitation has been measured for dopamine using time-resolved pump−probe techniques. The short-lived excited state suggests that internal conversion, intersystem crossing, and/or dissociation is a concern when ionizing at this wavelength using longer laser pulses. Photoionization of ion-beam-desorbed dopamine exhibits a large degree of fragmentation at all four wavelengths, though 267-nm photoionization produces the highest yield of dopamine fragment ions. Power dependence studies show a high degree of internal excitation. A direct comparison of ion yields obtained for photoionization of ion-beam-desorbed dopamine at 267 nm to that for SIMS shows a 20-fold increase in signal.

The behavior of gas-phase molecules when they interact with high-power femtosecond laser pulses is a topic of increasing interest due to emerging applications in mass spectrometry and surface analysis. With these lasers, it is possible to photoionize the target molecules with much higher efficiency than is possible using longer pulses, and there are several reports that suggest that the degree of photoinduced fragmentation is considerably reduced.[1−11] The reason for these effects is that, during resonance-enhanced multiphoton ionization, processes such as internal conversion and intersystem crossing to intermediate dissociative potential energy surfaces are avoided due to the very rapid optical pumping rate. With high molecular photoionization efficiency, it would be feasible to utilize mass spectrometry detection to assay trace levels of a wide variety of molecules.[12]

An especially relevant application involves the detection of neutral molecules desorbed from surfaces by energetic ion bombardment.[4,13] In the traditional mode, this experiment is performed by detection of ions formed directly during collisions between the primary ion and the sample surface, forming the basis of secondary ion mass spectrometry (SIMS). A large fraction of these desorbed species are, in fact, neutral and are not detected with SIMS measurements. If efficient laser photoionization methods are available, the neutral flux may be utilized in the analysis.[14−17] Efficient detection is critical in these experiments since the primary ion dose must be kept low enough to avoid measurable damage, limiting the amount of available sample.[18] Moreover, recent efforts at molecule-specific imaging have placed even more stringent requirements on the detection of desorbed molecules. For this situation, desorption occurs from a point on the surface of submicrometer size which contains less than 10^6 molecules.

The present generation of femtosecond lasers is capable of producing pulses ranging in wavelength from the UV to the IR

(1) Brummel, C. L.; Willey, K. F.; Vickerman, J. C.; Winograd, N. *Int. J. Mass Spectrom. Ion Processes* **1995**, *143*, 257−270.
(2) Willey, K. F.; Vorsa, V.; Braun, R. M.; Winograd N. *Rapid Commun. Mass Spectrom.* **1998**, 12, 1253−1260.
(3) Möllers, R.; Terhorst, M.; Niehuis, E.; Benninghoven, A. *Org. Mass Spectrom.* **1992**, 27, 1393−1395.
(4) Terhorst, M.; Möllers, R.; Niehuis, E.; Benninghoven, A. *Surf. Interface Anal.* **1992**, 18, 824−826.
(5) Ledingham, K. W. D.; Kosmidis, C.; Georgiou, S.; Couris, S.; Singhal, R. P. *Chem. Phys. Lett.* **1995**, 247, 555−563.
(6) Ledingham, K. W. D.; Singhal, R. P. *Int. J. Mass Spectrom. Ion Processes* **1997**, 163 149−168.
(7) Ledingham, K. W. D.; Singhal, R. P.; Smith, D. J.; McCanny, T.; Graham, P.; Kilic, H. S.; Peng, W. X.; Wang, S. L.; Langley, A. J.; Taday, P. F.; Kosmidis, C *J. Phys. Chem.* **1998**, *102*, 3002−3005.
(8) Smith, D. J.; Ledingham, K. W. D.; Kilic, H. S.; McCanny, T.; Peng, W. X.; Singhal, R. P.; Langley, A. J.; Taday, P. F.; Kosmidis, C *J. Phys. Chem.* **1998**, *102*, 2519−2526.
(9) Willey, K. F.; Brummel, C. L.; Winograd, N. *Chem. Phys. Lett.* **1997**, 267, 359−364.
(10) Grun, C.; Weickhardt, C.; Grotemeyer, J. *J. Eur. Mass Spectrom.* **1996**, 2, 197−202.
(11) Weinkauf, R.; Aicher, P.; Wesley, G.; Grotemeyer, J.; Schlag, E. W. *J. Phys. Chem.* **1994**, *98*, 8381−8391.
(12) Wood, M.; Zhou, Y.; Brummel, C. L.; Winograd, N. *Anal. Chem.* **1994**, *66*, 2425−2432.
(13) Winograd, N. *Anal. Chem.* **1993**, *65*, 622A−629A.
(14) Winograd, N.; Baxter, J. P.; Kimock, F. M. *Chem. Phys. Lett.* **1982**, 88, 581−584.
(15) Pappas, D. L.; Hrubowchak, D. M.; Ervin, M. H.; Winograd, N. *Science* **1989**, 243, 64−66.
(16) Becker, C. H.; Gillen, K. T. *Appl. Phys. Lett.* **1984**, 45, 1063−1065.
(17) Parks, J. E.; Schmitt, H. W.; Hurst, G. S.; Fairbank, W. M. *Thin Solid Films* **1983**, 108, 69−78.
(18) Benninghoven, A.; Sichtermann, W. *Anal. Chem.* **1978**, *50*, 1180−1184.

10.1021/ac980774m CCC: $18.00
Published on Web 12/18/1998

with peak power densities ranging from 10^6 to 10^{15} W/cm^2.[19,20] The mechanism of photoionization under these extreme conditions is under considerable discussion.[21−23] Although there is certainly evidence that traditional mechanisms such as resonance-enhanced multiphoton ionization (REMPI) are operative, other mechanisms, such as field ionization, have been proposed. Most importantly, however, the initial optimism surrounding the earliest photoionization observations has been tempered somewhat, since many molecules are still observed to undergo extensive fragmentation, even when interacting with ultrashort pulses, and especially when the power density is increased to achieve maximum ionization efficiency.[1,2,8,23]

In this paper, we examine the photoionization behavior of dopamine, both in the gas phase and when desorbed from a surface with an energetic ion beam. We have chosen to focus on this molecule since it is an aromatic molecule with a UV absorption near 270 nm.[25] Moreover, it also has a nonaromatic amine side chain which is readily subject to bond-cleavage reactions. Preliminary experiments suggested that, regardless of laser conditions, it is not possible to observe the molecular ion without concomitant fragmentation.[26] To resolve the mechanism of this fragmentation and to find ways to minimize it, we have examined the photoionization behavior as a function of wavelength, laser power density, and the amount of internal energy in the molecule. The results show that the major factor in controlling the nature of the photoionization spectrum is the amount of excess energy remaining in the molecular ion after absorbing the requisite number of photons to achieve ionization. Pump−probe experiments show that the lifetime of the $\pi-\pi^*$ intermediate sate is ∼10 ps. This short lifetime exposes a major point for potential fragmentation when using longer laser pulses by allowing internal conversion or intersystem crossing into nonbonding potential energy surfaces. Finally, we compare the ion yields obtained with femtosecond ionization of desorbed neutral dopamine with those obtained by SIMS and discuss the implications of the results for molecule-specific imaging experiments. In general, we find that photoionization with 267-nm radiation yields the highest number of characteristic ions. A degree of fragmentation is observed in all situations probed to date.

EXPERIMENTAL CONDITIONS

Photoionization experiments were carried out on a TOF−SIMS instrument described previously.[27] Briefly, high-energy (25 keV) Ga^+ ions produced by a liquid metal ion gun (LMIG) (Ionoptika) are directed at the sample, inducing desorption of ion and neutral species. The sample was prepared by pressing dopamine into a thin piece of In foil which was rolled flat onto the sample block. The sample block was then cooled to −125 °C in order to reduce the background signal caused by sublimation of the sample.[12] For SIMS experiments, the secondary ions formed at the sample surface are pulse extracted into a dual-field reflectron TOF mass analyzer by applying a positive potential (2.5 kV) directly to the sample stage. For laser photoionization experiments, charged particles produced at the surface are suppressed by setting the sample stage to a negative potential during ion bombardment. This voltage, of −1.2 kV, is applied at a time of several hundred nanoseconds prior to the primary ions striking the surface. Following ion bombardment, the sample stage is set to 2.5 kV. Several hundred nanoseconds later, the neutral species intersect the laser beam at a distance of 100−200 μm above the surface. The ensuing photoions are accelerated into the reflectron mass analyzer, where they are separated according to mass. This analyzer yields a mass resolution of 1 part in 3000 in the range $m/z = 20-200$.

Gas-phase photoionization experiments are performed by creating a pressure of 1×10^{-7} Torr of dopamine in the TOF−SIMS spectrometer. The molecules are introduced into the gas-phase by heating dopamine crystallites to ∼90 °C in vacuo, a temperature sufficiently high to allow a small degree of sublimation into the vacuum at the appropriate pressure. For this situation, the laser beam is directed through the extraction gap of 8 mm in size. The extraction voltage is set to +2.7 kV to allow the photoions to enter into the reflectron mass analyzer.

The Ti:sapphire femtosecond laser system (Clark-MXR, Inc.) employed in these experiments has been described previously.[1,2,9,28] Briefly, a self-mode-locked Ti:sapphire oscillator is pumped with 3 W from all emission wavelengths of an Ar^+ laser (Spectra Physics), generating 3-nJ, 50-fs pulses at 800 nm at a repetition rate of 100 MHz. Using chirped pulse amplification techniques, these pulses are first stretched to ∼300 ps before entering a Ti:sapphire regenerative amplifier operating at 1 kHz. The pulses are amplified to ∼1.6 mJ and are then sent into a postamplifier,[1,28] where they are amplified further to 5.5 mJ. The pulses are finally compressed to ∼100 fs in a grating-based compressor. The final output is a 1-kHz train of pulses at a wavelength of 800 nm and containing ∼3.5 mJ of energy per pulse at a pulse width of ∼100 fs. The 800-nm output is either used directly or sent into a harmonic generator to produce additional wavelengths at 400, 267, or 200 nm.[2] An upper limit of 230 fs was measured for the 267-nm beam by cross-correlation with the 800-nm beam. The cross-correlation width is obtained by measuring the ion signal arising from short-lived molecular states as a function of temporal overlap between the 267- and 800-nm laser pulses. Using the same cross-correlation method, an upper limit of 400 fs was measured for the 200-nm beam. The pulse width of the second harmonic has not been measured directly but should be no greater than that of the third harmonic. The laser is coupled into the analysis chamber with a 30-cm focal length CaF_2 lens. The laser spot size and position over the sample are controlled by movement of this lens mounted on an *x*,*y*,*z* manipulator outside the chamber. By changing the laser pulse energy and focal dimensions, the laser power density (measured in W/cm^2) in the

(19) Perry, M. D.; Mourou, G. *Science* **1994**, 264, 917−924.
(20) Backus, S.; Durfee, C. G., III; Murnane, M. M.; Kapteyn, H. C. *Rev. Sci. Instrum.* **1998**, 69, 1207−1223.
(21) Conjusteau, A.; Bandrauk, A. D.; Corkum, P. B. *J. Chem. Phys.* **1997**, 106, 9095−9104.
(22) DeWitt, M. J.; Levis, R. J. *J. Chem. Phys.* **1995**, *102*, 8670−8673.
(23) DeWitt, M. J.; Levis, R. J. *J. Chem. Phys.* **1998**, *108*, 7045−7048.
(24) DeWitt, M. J.; Levis, R. J. *J. Chem. Phys.* **1998**, *108*, 7739−7742.
(25) Li, L.; Lubman, D. M. *Anal. Chem.* **1987**, *59*, 2538−2541.
(26) Willey, K. F.; Brummel, C. L.; Winograd, N. In *Secondary Ion Mass Spectrometry (SIMS X)*; Benninghoven, A., Hagenhoff, B., Werner, H. W., Eds.; Wiley and Sons: New York, 1996; pp 797−800.
(27) Braun, R. M.; Blenkinsopp, P.; Mullock, S. J.; Corlett, C.; Willey, K. F.; Vickerman, J. C.; Winograd, N. *Rapid Commun. Mass Spectrom.* **1998**, *12*, 1246−1252.
(28) Dugan, M. A.; Pacholski, M. L.; Willey, K. F.; Braun, R. M.; Winograd, N. In *Resonance Ionization Spectroscopy 1996: Eighth International Symposium*; Winograd, N., Parks, J. E., Eds.; AIP Press: Woodbury, NY, 1997; pp 423−426.

extraction region may be varied over several orders of magnitude. For power-dependent studies, the laser spot size is fixed, and the energy is attenuated using reflective neutral density filters to vary the intensity. The power density is calculated by dividing the energy for a single pulse by the area of the laser beam at the interaction region and the pulse width. This procedure has been described previously.[1]

For time-resolved experiments, the pump beam is produced from the third harmonic (267 nm), and the probe beam is generated by picking off ~10% of the fundamental before it enters the harmonic generator. The pump beam travels a fixed delay path, while the probe beam travels a manually controlled variable delay path to the chamber. The two beams are then combined with a dichroic mirror and directed through the 30-cm focal length CaF_2 lens into the chamber. The beam sizes of the pump and probe at the interaction region are ~500 and ~700 μm, respectively. The laser power density of each beam is adjusted to minimize any signal arising from one beam only. The power densities were $\sim 6 \times 10^{10}$ and 9×10^{11} W/cm^2 per pulse for the pump and probe beams, respectively. The electric field vectors for both the pump and probe beams are parallel to each other.

Different detectors are required for gas-phase photoinization experiments and for ion-beam-induced desorption experiments due to the different signal levels involved. In the gas phase, large signal levels require analog detection. To achieve this mode, the signal is capacitively coupled from the detector to analog processing electronics and then sent to a digital-to-analog converter (DA500, Signatec) with 2-ns time resolution. Power dependence data are collected in triplicate using a total of 15 000 laser shots for each point. The time-resolved data are acquired with 20 000 shots for each data point. Conversely, ion-beam desorption and SIMS experiments generate signal levels in the single-ion-counting regime. Here, each ion pulse is sent through a ×4 preamplifier and a discriminator. The output of the discriminator is sent to a time-to-digital converter (model 9805, Precision Instruments Inc.) with 1-ns time resolution. Each spectrum is acquired by averaging four spectra from 50 000 laser pulses or ion pulses.

RESULTS AND DISCUSSION

Here we examine the photoionization of dopamine by femtosecond laser pulses of various wavelengths. Of special interest is to compare the degree of fragmentation that is observed in the gas phase at room temperature with that desorbed from surfaces by an energetic ion beam. This comparison is important to make since the ion-beam-desorbed molecules are known to have more internal energy than molecules formed by thermal evaporation. The photoionization and fragmentation patterns of gas-phase dopamine at 800, 400, 267, and 200 nm are presented first. Power dependence studies are employed to elucidate the possible fragmentation mechanisms of dopamine upon photoexcitation. Time-resolved results are detailed which provide excited-state lifetime information of dopamine following 267-nm excitation. Next, ion yields, fragmentation patterns, and power dependencies of photoionized dopamine which has been desorbed from a surface by energetic ion bombardment are determined in order to establish the role of excess internal energy in photodissociation processes. Finally, ionization yields of the various photoproducts are compared to ionization yields with SIMS to assess the relative analytical capabilities of the two approaches.

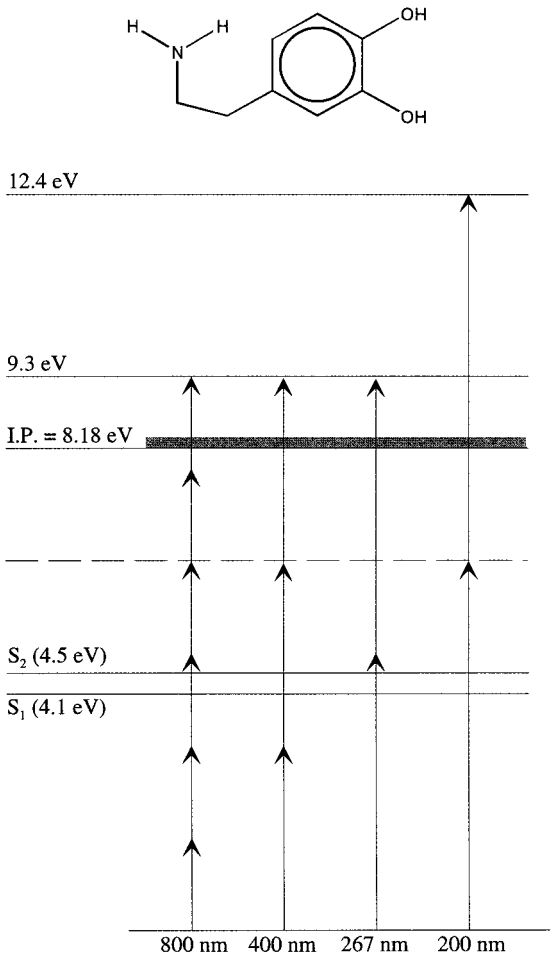

Figure 1. Schematic electronic energy diagram and multiphoton ionization schemes for dopamine. The energy information is taken from ref 29. The vertical arrows depict the minimum number of photons required for ionization at each wavelength. Gas-phase dopamine exhibits a strong absorption band around 200 nm (dashed line) (ref 25).

Photoionization of Gas-Phase Dopamine. The minimum number of photons required to ionize dopamine (IP, 8.18 eV)[29] with 800, 400, 267, and 200 nm is 6, 3, 2, and 2, respectively, as shown in Figure 1. These wavelengths lead to a total excitation energy of 9.3 eV or an excess energy of 1.1 eV available for the ion state for the three longer wavelengths. Absorption of two 200-nm photons, on the other hand, leaves an excess energy of 4.2 eV. Franck−Condon factors of the excited and ionic molecular states dictate that this excess energy be partitioned into kinetic energy of the ejected electron and the excited ionic states. Since neither the molecular energies nor the shape of the potential curves for cationic dopamine is known, it is difficult to predict how much of this excess energy will reside in the molecular ion or in the kinetic energy of the ejected electron. Some information pertinent to ground-state dopamine is known, however. The UV−visible absorption spectra[25] exhibit broad peaks around 200 and 267 nm. An energy separation of 4.1 eV between the S_0 ground state and the S_1 first excited state has also been reported.[29]

The dopamine mass spectrum following femtosecond photoionization taken at near-threshold laser conditions for the four

(29) Choi, Y.; Lubman, D. M. *Anal. Chem.* **1992**, *64*, 2726−2734.

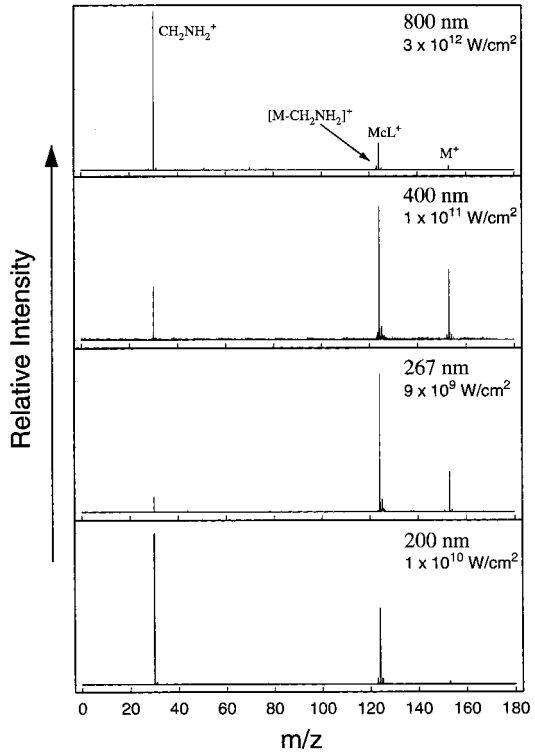

Figure 2. Near-threshold femtosecond ionization−dissociation mass spectra for gas-phase dopamine illustrating the relative ion yields for 800-, 400-, 267-, and 200-nm excitation. The molecular ion at m/z = 153 is denoted as M^+. The m/z = 124 peak is a fragment resulting from a McLafferty rearrangement reaction (see text) and is denoted as McL^+. Two other ion channels are observed at m/z = 30 and 123 and correspond to the aminomethyl cation ($CH_2NH_2^+$) and $[M - CH_2NH_2]^+$.

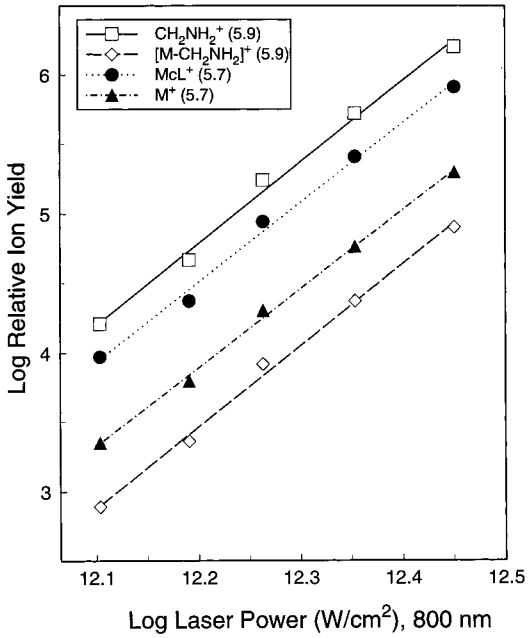

Figure 3. Relative product ion yield of gas-phase dopamine as a function of laser power density at 800 nm. The measured photon order is given in parentheses for each product ion.

wavelengths is shown in Figure 2. Three major and one minor ion channels are observed. The highest mass, at m/z = 153, corresponds to the intact molecular ion (M^+). Two fragment ion channels are observed which originate from the α-cleavage of the C−C bond in the alkyl chain portion of the molecule. The most intense of these two peaks is at m/z = 30, corresponding to the aminomethyl cation, $CH_2NH_2^+$. The corresponding neutral radical of this species has an especially low ionization potential of 6.7 eV.[30] The much weaker fragment ion channel, at m/z = 123, corresponds to $[M - CH_2NH_2]^+$. The other major fragment ion, at m/z = 124, does not arise from any direct dissociation process, but stems from an ion rearrangement reaction (see below). Photoionization at 800 nm exhibits fragmentation mostly into the $CH_2NH_2^+$ channel. Near-threshold ionization with 400 and 267 nm yields m/z = 124 as the dominant channel and a larger branching ratio into the M^+ channel than into the $CH_2NH_2^+$ channel. Photoionization at 200 nm produces mostly the m/z = 30 and 124 ions and very little M^+.

The m/z = 124 ion most likely arises from a radical site rearrangement reaction. This type of rearrangement is frequently seen in the electron impact mass spectra of phenylalkanes where the side chain is propyl or larger[31] and is commonly referred to as a McLafferty rearrangement. We shall denote this ion as McL^+. In this reaction, a radical site is formed on the aromatic ring, followed by a hydrogen rearrangement and an α-site cleavage. It is important to stress that this reaction takes place in the ion state rather than in the neutral state as

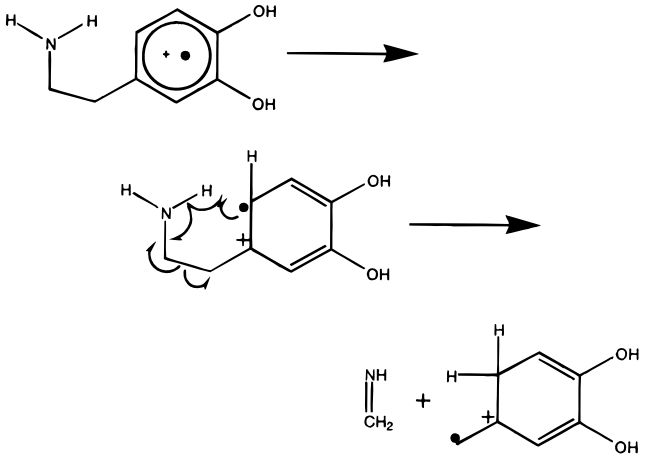

The power dependence for each ion channel at 800 nm for power densities up to ~3×10^{12} W/cm^2 is shown in Figure 3. No evidence of saturation of the ionization volume (ionization of a large fraction of species in the laser beam) is observed for any of the product ions. However, saturation of an individual electronic transition cannot be ruled out. The measured photon orders with standard errors are given in Table 1. It is not currently possible to interrogate a broader laser power density range due to the high photon orders that are involved. A decrease of a factor of 2 in laser power density, for example, results in a 64-fold decrease in signal for a six-photon process. The photon orders of all four ion channels are similar, which indicates that the fragmentation must be occurring in the ion state rather than in the neutral state.

(30) Lias, S. G.; Bartmess, J. E.; Liebman, J. F.; Holmes, J. L.; Levin, R. D.; Mallard, W. G. *J. Phys. Chem. Ref. Data, Suppl. 1* **1988**, *17*, 1−861.
(31) McLafferty, F. W.; Turecek, F. *Interpretation of Mass Spectra*, 4th ed.; University Science Books: Sausalito, CA, 1993; p 239.

Table 1. Photon Orders with Standard Errors for the Four Ion Channels Following Photoionization of Gas-Phase Dopamine at 800, 400, and 267 nm[a]

λ (nm)	(nm) photon order				range (W/cm^2)
	m/z 30	m/z 123	m/z 124	m/z 153	
800	5.9 ± 0.3	5.9 ± 0.2	5.7 ± 0.3	5.7 ± 0.2	$1 \times 10^{12}-3 \times 10^{12}$
400	3.5 ± 0.1	3.8 ± 0.3	2.8 ± 0.1	2.8 ± 0.1	$5 \times 10^{10}-5 \times 10^{11}$
267	2.3 ± 0.1	2.8 ± 0.2	1.8 ± 0.1	1.9 ± 0.1	$6 \times 10^{9}-2 \times 10^{11}$

[a] The laser power density range for each wavelength is also listed.

An analogous power dependence of dopamine at 400 nm was performed for laser power densities up to 4×10^{11} W/cm^2. At least three photons are required to ionize dopamine at 400 nm. Unlike the situation for 800-nm excitation, the ion channels here exhibit varying photon orders (see Table 1). The molecular ion and the $m/z = 124$ peak each exhibit a photon order of 2.8. The $m/z = 30$ and 123 fragments exhibit a higher photon order of 3.5 and 3.8, respectively. No evidence of saturation of the ionization volume is observed for any of the product ions in the power density range studied.

The power dependence of dopamine at 267 nm was carried out in the laser power density range of $6.3 \times 10^{9}-1.5 \times 10^{11}$ W/cm^2. The behavior is similar to the situation at 400 nm, in that the $m/z = 124$ and 153 channels exhibit similar power dependencies with slopes of 1.8 and 1.9, respectively, while the $m/z = 30$ and 123 channels exhibit power dependencies with higher photon orders of 2.3 and 2.8, respectively. The photoionization mechanisms for 400- and 267-nm excitation appear to be qualitatively similar to each other. Photon orders for all three wavelengths including standard errors are summarized in Table 1. Power dependencies for 200-nm photoexcitation are not included due to the small laser power density range available for this experiment.

One question that arises immediately is, why do each of the 800-nm product ions display a uniform power dependence, while 400- and 267-nm product ions do not? Initially, it may appear that, for 800-nm excitation, an ionization followed by dissociation (ID) mechanism[8] is operative with six photons, while for 400- and 267-nm excitation, additional photons may be absorbed in the ion state which lead to the differing branching ratios. Since the minimum accessible energy above the ionization potential is 9.3 eV for all three wavelengths, we would expect the product ion distributions to be similar at threshold laser power densities. However, 800-nm excitation produces the $CH_2NH_2^+$ as the dominant product. On the other hand, 400- and 267-nm excitations show the $CH_2NH_2^+$ channel becoming dominant only at higher power densities. This result suggests that more than six photons are being absorbed by dopamine with 800-nm excitation and that at least one step in the absorption ladder is saturated since the power dependence study indicates a photon order of 6. At higher laser power densities ($10^{12}-10^{13}$ W/cm^2), the 400-nm power dependence experiments exhibit similar behavior. In this higher intensity study, the $CH_2NH_2^+$ ion is the dominant mass peak, exhibiting a measured photon order of ~3, thus indicating saturation.

Fragmentation of neutral dopamine followed by ionization of the fragments (DI)[8] is unlikely due to the ultrashort time scale of the excitation pulses (see below). However, the presence of high-intensity laser pulses raises the concern of field or tunnel ionization mechanisms.[6] A qualitative criterion for field ionization that has been applied to atoms[32,33] and molecules[21-24] is the Keldysh parameter,[34]

$$\gamma = \left[\frac{\mathrm{IP}}{(1.87 \times 10^{-13})\, I\lambda^2}\right]^{1/2}$$

where IP is the ionization potential, I is the laser power density in W/cm^2, and λ is the wavelength in μm. MPI is believed to dominate when $\gamma \gg 1$, and field ionization prevails for $\gamma \ll 1$. For $\gamma < 0.5$, tunneling ionization (TI) is believed to occur.[24,35,36] In the 800-nm study presented here, the Keldysh parameter varies from 5 (3×10^{12} W/cm^2) to 11 (1×10^{12} W/cm^2). It appears unlikely that these mechanisms are operative here, but since these values are in the intermediate regime, TI and field ionization cannot be definitely ruled out.

Finally, we examine the photoionization behavior at 200 nm where the dopamine molecular ion is potentially left with up to 4.2 eV of excess energy. As is evident from Figure 2d, the relative product ion yields are 51, 3, 44, and 2% for the $m/z = 30$, 123, 124, and 153 channels, respectively. These branching ratios remain the same for laser power densities down to $\sim 4 \times 10^9$ W/cm^2. These observations strongly suggest that the extensive fragmentation results from the large amount of excess energy caused by the two-photon absorption, promoting fragmentation of the molecule.

At this stage, it appears that excess energy deposited into the molecule by multiphoton absorption is the dominant factor in influencing the degree of fragmentation. This idea is supported by an earlier photoionization experiment on dopamine in the nanosecond time domain. Lubman and co-workers examined photoionized jet-cooled dopamine using nanosecond resonant two-photon ionization at 280 nm.[37,38] The only observed peak in the mass spectrum is that of the molecular ion. Excitation at 280 nm results in 0.68 eV of excess energy, whereas excitation at 800, 400, and 267 nm excitation yields 1.1 eV of excess energy. While jet-cooling may help reduce the degree of fragmentation, this excess energy difference is the most likely cause of the observed difference in fragmentation, especially considering that bond energies are usually much lower in the ion state than in the ground state. Although a wavelength dependence was not performed for dopamine, related studies have been reported for tyramine.[38] Tyramine, which differs from dopamine only in the absence of the meta hydroxyl group, exhibits a strong fragmentation dependence with wavelength. At 280 nm, there is very little fragmentation, while at 222 nm fragmentation channels are dominant. Moreover, ionization at two intermediate wavelengths (266 and 245 nm) indicates there is a gradual, rather than abrupt, onset of fragmentation.

(32) Augst, S.; Meyerhofer, D. D.; Strickland, D.; Chin, S. L. *J. Opt. Soc. Am. B* **1991**, *8*, 858−867.
(33) Krainov, V. P.; Shokri, B *Sov. Phys. JEPT* **1995**, *80*, 657−661.
(34) Keldysh, L. V. *Sov. Phys. JETP* **1965**, *20*, 1307−1316.
(35) DeWitt, M. J.; Levis, R. J. *J. Phys. Chem. B* **1998**, *102*, 13272−13279.
(36) Kosmidis, C.; Ledingham, K. W. D.; Kilic, H. S.; McCanny, T.; Singhal, R. P.; Langley, A. J.; Shaikh, W. *J. Phys. Chem.* **1997**, *101*, 2246−2270.
(37) Lubman, D. M. In *Lasers and Mass Spectrometry*; Lubman, D. M., Ed.; Oxford University Press: Oxford, U.K., 1990; pp 353−382.
(38) Tembreull, R.; Lubman, D. M. *Anal. Chem.* **1987**, *59*, 1082−1088.

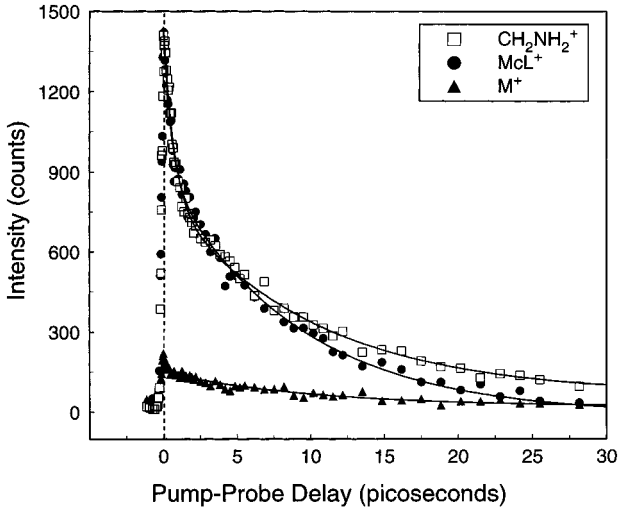

Figure 4. Time-resolved product ion dependence of gas-phase dopamine following 267-nm excitation (pump) and 800-nm ionization (probe). The relative pump−probe polarization is parallel. The solid lines are a result of biexponential fits to the data. The measured time constants of the fast component for $CH_2NH_2^+$, McL^+, and M^+ are 0.76 ± 0.06, 0.58 ± 0.06 and 0.18 ± 0.04 ps, respectively. The measured time constants of the slow component are 10.07 ± 0.62, 8.95 ± 0.44 and 10.06 ± 0.78 ps, respectively. The time dependence of the $m/z = 123$ channel is not plotted due to extremely low signal levels.

267-nm Excited-State Lifetime of Dopamine. To avoid fragmentation during the formation of the molecular ion, the lifetime of the intermediate states in the multiphoton absorption ladder should be long with respect to the length of the laser pulse and the optical pumping rate.[11] It is possible to measure these lifetimes by pumping the optical absorption at 267 nm, followed by probing with a delayed 800-nm femtosecond laser pulse. As noted earlier, a broad absorption band has been reported for gas-phase dopamine peaking at approximately 270 nm.[25] Excitation at 267 nm results in a $\pi-\pi^*$ transition involving the phenyl portion of the molecule. The energy of this transition (4.65 eV) is consistent with excitation into the S_1 (4.1 eV) or S_2 (4.5 eV) states of this molecule.[29] Ionization of dopamine following 267-nm excitation requires an additional 3.5 eV, which corresponds to three photons at 800 nm.

The time-dependent signal for the three major ion channels following 267-nm excitation is shown in Figure 4. Signal arising from pump and probe pulses individually is eliminated by reducing the laser power density for both beams to a value just below the threshold for ion formation. The $m/z = 123$ time dependence is not plotted due to the fact that the signal levels are not adequately measurable. The three major ion channels exhibit essentially the same time-dependent behavior, with the peak in ion intensity occurring at zero pump−probe delay. The ion signal initially decays to ~70% of the maximum in less than 1 ps, followed by a slower decay on a time scale of ~10 ps. Both decay times were obtained by fitting the data to a biexponential decay.

The ion channels all yield maximum signal at zero pump−probe delay, indicating that both the $CH_2NH_2^+$ and McL^+ rearrangement fragment ions are formed following ionization of the parent molecule as opposed to a DI mechanism. If any of these fragments are formed via a DI mechanism, we would then expect to see a peak shift of the signal maximum to positive delay times for that fragment ion. Moreover, all channels exhibit a similar decay rate, which strongly indicates that they originate from the same parent ion. The fast decay component is most likely due to rotational dephasing of the initially excited dopamine since the data were recorded using parallel pump and probe beams, rather than at the magic angle.[39,40] The slower component appears to arise from an internal conversion from the S_1 or S_2 excited states to the S_0 ground state of the molecule. Similar rates (~10 ps) have been observed for the internal conversion from S_1 to S_0 in benzene.[41] The decrease in signal is due to an unfavorable Franck−Condon overlap between high vibrational states of S_0 and ion states of the molecule. The longer decay time for all three channels yields a 267-nm excited-state lifetime on the order of ~10 ps. As mentioned earlier, nanosecond photoionization of dopamine at 280 nm produces only molecular ion signal at threshold laser power densities.[37,38] We believe the major differences between the two spectra are due to the lifetime of the intermediate state as a function of vibrational energy and the amount of excess energy in the ion state following ionization.

Photoionization of Ion-Beam-Desorbed Dopamine. With the mass spectra of gas-phase dopamine well-characterized at the available wavelengths and power densities, we next examine how these spectra differ for dopamine desorbed from a surface by energetic ion bombardment. These spectra will presumably be more complicated to interpret since some of the dopamine molecules will be fragmented during the desorption process and there will be a broader range of internal energies associated with all of the desorbed species. The mass spectra of dopamine taken at near threshold laser power density are shown in Figure 5. A much higher degree of fragmentation and spectral congestion (particularly at lower masses) is observed in these spectra than in the corresponding gas-phase spectra. The dominant peak at all excitation wavelengths and laser power densities is $CH_2NH_2^+$. The $m/z = 123$ and 124 fragments are both present, although the yield of the $m/z = 123$ ion is much greater than that of the $m/z = 124$ ion. This important observation strongly suggests that the $m/z = 123$ species arises from direct photoionization of a neutral fragment of dopamine formed during the desorption process. Otherwise, we would expect a significant contribution from the McL^+ fragment at $m/z = 124$. Moreover, although the molecular ion is present, its yield is low (<1% of the characteristic fragments). Finally, a group of fragment ions are observed in the range of $m/z = 149-153$. These species have lost one or more hydrogen atoms from the parent molecule. The largest yield of ions in this group of peaks (including the molecular ion) is the $m/z = 151$ species.

With 267-nm excitation, there is one fragment at $m/z = 136$ that is not observed in the gas-phase spectra, as can be seen in Figure 5. This m/z value corresponds to a loss of 17.026 ± 0.006 amu and arises from the loss of an NH_3 group from the dopamine molecule. We have ruled out the possibility that this mass difference might be attributable to the loss of an OH group not only from the exact mass analysis (OH loss occurs with $m/z =$

(39) Scherer, N. F.; Khundkar, L. R.; Rose, T. S.; Zewail, H. H. *J. Phys. Chem.* **1987**, *91*, 6478−6483.
(40) Fuss, W.; Schikarski, T.; Schmid, W. E.; Trushin, S. A.; Hering, P.; Kompa, K. L. *J. Chem. Phys.* **1997**, *106*, 2205−2211.
(41) Radloff, W.; Stert V.; Freudenberg, T.; Hertel, I. V.; Jouvet, C.; Dedonder-Lardeux, C.; Solgadi, D. *Chem. Phys. Lett.* **1997**, *281*, 20−26.

Table 2. Photon Orders with Standard Errors for the Various Ion Channels Following Photoionization of Ion-Beam-Desorbed Dopamine at 800, 400, 267, and 200 nm[a]

λ (nm)	photon order					range (W/cm^2)
	m/*z* 30	*m*/*z* 123	*m*/*z* 124	*m*/*z* 136	*m*/*z* 153	
800	2.4 ± 0.1	2.5 ± 0.1	2.5 ± 0.1	–	1.7 ± 0.1	1×10^{12}–8×10^{12}
400	2.27 ± 0.03	2.14 ± 0.03	2.2 ± 0.1	–	1.6 ± 0.1	1×10^{11}–2×10^{12}
267	1.7 ± 0.1	1.4 ± 0.1	1.6 ± 0.1	1.3 ± 0.1	1.4 ± 0.1	3×10^{10}–5×10^{11}
200	1.7 ± 0.1	1.5 ± 0.1	1.6 ± 0.1	1.6 ± 0.2		1×10^{11}–2×10^{12}

[a] The laser power density range for each wavelength is also listed.

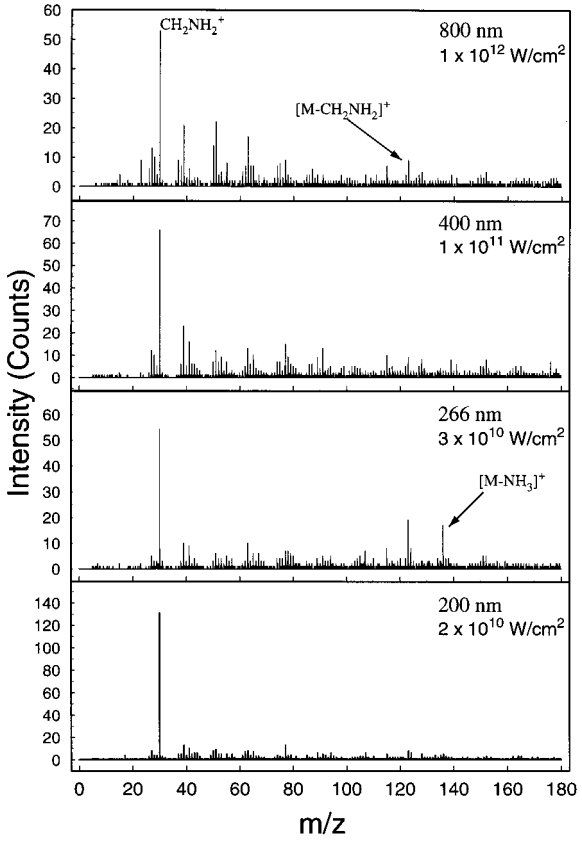

Figure 5. Femtosecond photoionization mass spectra of ion-desorbed dopamine obtained with 800-, 400-, 267-, and 200-nm excitation.

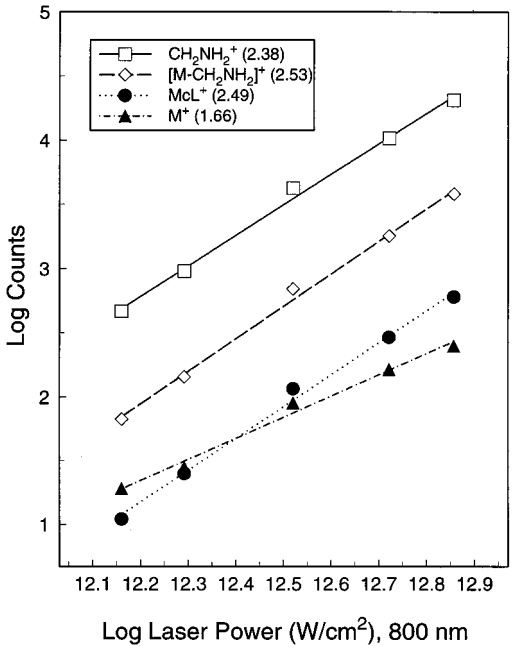

Figure 6. Relative photoionization fragment ion yield as a function of laser power density at 800 nm for characteristic dopamine fragments.

17.003) but also by comparison to the photoionization spectrum of phenethylamine. Phenethylamine is identical to dopamine except for the absence of the two hydroxyls on the phenyl ring. The molecular weight of phenethylamine is 121 amu, and therefore, a loss of [NH_3] would result in a fragment peak at $m/z = 104$. In fact, a relatively strong peak at $m/z = 104$ is observed.

To gain insight into the origin of these fragment ions, power dependence studies using laser power densities similar to those reported for gas-phase studies were completed. The result for 800-nm photoionization is shown in Figure 6, and the photon orders for all four wavelengths are summarized in Table 2. The dominant peak at all wavelengths and intensities is the $CH_2NH_2^+$ ion. Moreover, the relative yields of M^+ and McL^+ are very low for the ion-desorbed species.

The measured photon orders as reported in Table 2 are consistently lower than those observed in the gas phase. The 267- and 200-nm power dependencies, for example, exhibit photon orders lower than 2. It is possible that this effect is due to saturation of the π–π^* excitation or other unknown transitions. In this case, the expected photon order at low power density would be higher than the photon order at high power density. The slopes reported in all the figures exhibit no such trend. Saturation of the ionization volume is also an issue. We believe this phenomenon is not effecting our data since the range of power densities is similar to those employed in the gas-phase experiments, where no saturation of the ionization volume is observed. These observations, then, suggest that the ion-beam desorption process is producing species with a high degree of vibrational and electronic excitation. This high degree of excitation is reflected in the lower number of photons needed to ionize the ion desorbed species. The results also show photon orders far from integer values for all the characteristic species at the four wavelengths. The noninteger orders are characteristic of a distribution of internal energies.

Ion-Beam-Desorbed versus SIMS Ion Yields. It is of interest to compare directly the photoionization spectrum of ion-desorbed dopamine with the corresponding dopamine SIMS spectrum. This comparison should yield insight into which ions most easily form during the desorption process itself. In addition, it is useful to compare the relative number and type of ions formed

Table 3. Absolute Ion Yield for Each Characteristic Ion Channel Obtained with 267-nm Photoionization and SIMS[a]

	abs ion yield							
	m/z 30	*m/z* 123	*m/z* 124	*m/z* 136	*m/z* 137	*m/z* 153	*m/z* 154	total
photoionization	110993	6591	6806	3794	–	716	–	128900
SIMS	3839	216	138	–	1670	–	595	6458

[a]Total ion dose for each experiment was 4.4×10^{11} Ga^+/cm^2. The laser spot size was ~175 μm, and the intensity was set to 7.3×10^{11} W/cm^2.

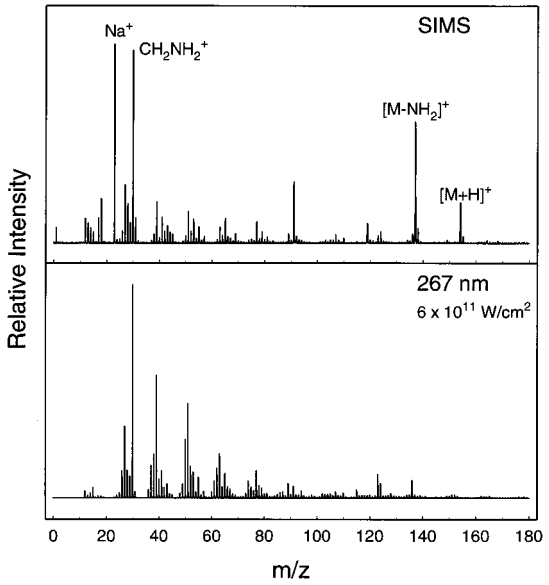

Figure 7. TOF–SIMS and 267-nm photoionization mass spectra of ion-desorbed dopamine.

by both methods for purely analytical purposes. The positive ion SIMS spectrum is shown in Figure 7. The base peak in the spectrum is Na^+, a ubiquitously observed peak in SIMS due to its high ionization efficiency. Major fragments are found at m/z = 30, 137, and 154. The largest of the fragment peaks is $CH_2NH_2^+$, as is found for the laser ionization experiments. The quasi molecular ion is observed at m/z = 154 $(M + H)^+$. The m/z = 123 and 124 peaks are observed, but at much lower signal levels (<1%) than the three major peaks. In addition, there is a relatively strong peak at m/z = 91 assigned to $C_7H_7^+$ from rearrangement of the aromatic ring. Finally, there is a strong peak at m/z = 137 which arises from the loss of $-NH_3$ from $(M + H)^+$. This pathway is also seen in the photoionization spectrum of ion-desorbed dopamine, but not in the gas-phase spectra.

The total number of ions emerging from the laser photoionization experiments generally exceeds that observed by SIMS, as shown in Table 3 and Figure 7, where the ion yields are compared for identical ion-bombardment conditions. To achieve these results, the laser beam is focused to a size of ~175 μm and is positioned 250 μm above the sample, where the intensity is ~7 $\times$ 10^{11} W/cm^2. Note that the total number of characteristic fragment ions is 20-fold higher with laser ionization compared to that with SIMS. Most of this gain, however, arises from the increased yield of the $CH_2NH_2^+$ fragment. After excluding the $CH_2NH_2^+$ ion from the summation, there is still a 7-fold increase in signal. The intensity of the intact dopamine neutral molecule obtained using laser postionization is similar to that found using SIMS.

CONCLUSIONS

We have carried out femtosecond photoionization studies of dopamine in the gas phase and desorbed from a surface by kiloelectronvolt ion bombardment at wavelengths of 800, 400, 267, and 200 nm. The molecular ion is observed in the gas phase at m/z = 153 along with three fragment ions at m/z = 30, 123, and 124. The $CH_2NH_2^+$ and $[M - CH_2NH_2]^+$ fragments result from cleavage of the C–C bond in the alkyl chain. The m/z = 124 ion results from a radical site rearrangement reaction in which a hydrogen atom from the alkyl chain is transferred to the phenyl portion of the molecule. Using ultrafast pump–probe techniques, the excited-state lifetime of gas-phase dopamine following 267-nm excitation has been measured to be ~10 ps. This energy ends up either in highly excited vibrational states through internal conversion, which is then transferred into the ion state following photoionization, or in dissociation of the neutral molecule. Ion-desorbed dopamine is found to undergo extensive fragmentation, and the fragments are found to contain a high degree of internal excitation. This conclusion is supported by power dependence studies which show that photon orders are considerably lower than those seen in gas-phase studies at similar power densities. Excitation with 267 nm produces the largest ion yields of characteristic dopamine fragments. A direct comparison of the yields obtained for photoionization of ion-beam-desorbed dopamine to that for SIMS has been made. We find that a 20-fold increase in signal is possible for fragment molecules, allowing surface analysis studies of the desorbed neutral species. Moreover, experiments are currently underway which incorporate femtosecond photoionization with molecule-specific imaging of biological surfaces. Imaging requires that surface molecules be transported to the detector with maximum possible efficiency due to the small number of desorbed species.

ACKNOWLEDGMENT

The support of the National Institutes of Health and the National Science Foundation for partial funding of this work is gratefully acknowledged.

Received for review July 14, 1998. Accepted October 20, 1998.

AC980774M